Magnetic phases in iron-doped $NiCl_2$

1991 J. Phys.: Condens. Matter 3 5741

(http://iopscience.iop.org/0953-8984/3/30/007)

J. Phys.: Condens. Matter 3 (1991) 5741–5750. Printed in the UK

Magnetic phases in iron-doped $NiCl_2$

R J Pollard†, C Bauer†, J Laban‡, and V H McCann‡

† Department of Physics, Monash University, Clayton, Victoria 3168, Australia
‡ Department of Physics, University of Canterbury, Christchurch, New Zealand

Received 21 January 1991, in final form 17 April 1991

Abstract. The magnetic phases of two concentrations of iron in $Fe_xNi_{1-x}Cl_2$ ($x = 0.06$ and 0.10) are reported from ^{57}Fe Mössbauer spectroscopy. Published date were used for $x = 0.06$, and new data are presented for $x = 0.10$. Substituting $x = 0.10$ causes the ferrous moments to align along the crystallographic c-axis, whereas in pure $NiCl_2$ the moments are perpendicular to the c-axis. For $x = 0.06$ parallel and perpendicular phases coexist, with the proportion of parallel moments decreasing smoothly from 74% at 4.2 K to zero at the Néel temperature (T_N). The introduction of iron reduces T_N from 52 K ($x = 0$) to 46 K ($x = 0.10$). A crystal field model was used to interpret temperature variations of the hyperfine parameters. The effective magnetic exchange constant for parallel moments is twice as large as that for perpendicular moments. In addition the Fermi contact constant B_c is -50 T for parallel moments, compared with 40 T for perpendicular moments. A 6 T magnetic field applied along the c-axis for $x = 0.10$ at 5 K induces a canting of the moments from the principal electric field gradient axis by 20–35°, and it is inferred that under these conditions the system is in a spin-flopped state in which the ferrous ions experience nearly identical environments.

1. Introduction

Magnetic systems in which determinants of the ordered state compete with comparable magnitude have been of interest for over a decade, and have permitted a testing of theoretical predictions. For systems with two orthogonal spin anisotropies, three ordered phases are expected depending on the composition and temperature. In two of the phases the spins are all aligned along one of the anisotropy axes (denoted by $S_\parallel$ and $S_\perp$), and the third intermediate phase is either mixed or oblique antiferromagnetic [1, 2].

In a mixed phase the relative proportions of parallel and perpendicular spins should vary with temperature, whereas in an oblique phase the moments of both types of magnetic ions are canted with respect to the axes and the canting angle varies with temperature. Microscopic details of the intermediate phase can be determined from Mössbauer experiments; reports on a number of systems have supported oblique alignment [1, 2].

The $Fe_xNi_{1-x}Cl_2$ system has been studied by Ito and co-workers using neutron scattering [3], Mössbauer spectroscopy [3, 4] and magnetization measurements [5]. The crystal structure is of the $CdCl_2$-type, in which the magnetic ions lie in hexagonal layers which are separated by two close-packed layers of Cl^- ions. The magnetic ions experience a large potential of cubic symmetry and a smaller potential of trigonal

0953-8984/91/305741+10$03.50

symmetry. The trigonal S_6 axis is along the c-axis, perpendicular to the plane of the layers. Consequently in the paramagnetic state the electric field gradient tensor (EFG) is axially symmetric and its principal component (V_{zz}) is along the c-axis. In a magnetically ordered state the EFG is affected by the magnetization, and in general V_{zz} is tilted away from the c-axis at an angle which depends on the spin direction and which varies with temperature [6].

The spin anisotropies are orthogonal: referring to directions with respect to the c-axis, Fe^{2+} provides a strong parallel anisotropy ($S_\parallel$) and Ni^{2+} provides a weak perpendicular anisotropy ($S_\perp$) [2, 6]. Hence the moments are perpendicular to the c-axis for low iron concentrations [6], and are expected to be parallel to the c-axis for high concentrations [2].

The neutron experiments were used to draw a magnetic phase diagram in which the mixed or oblique phase is located in a concentration region between $x = 0.01$ and 0.12 at [3]. According to the diagram, raising the temperature in this concentration range leads to a transition to an ordered perpendicular phase (at 40 K for $x = 0.06$) and then to paramagnetism (at 50 K for $x = 0.06$). The tetracritical point is at $x = 0.12$; for $x > 0.12$ there is only one ordered phase ($S_\parallel$) and T_N gradually decreases with increasing x.

Mössbauer measurements have been performed on the same samples used for the neutron experiments, and high quality spectra for $x = 0.06$ were published [3]. The researchers were unsuccessful in satisfactorily analysing the spectra, however the angle θ_{hf} between the internal magnetic field and V_{zz} was estimated. At 4.2 K θ_{hf} appeared to change gradually from 90° for $x \simeq 0.01$ to 0° for $x \simeq 0.1$. For $x = 0.06$ at 4.2 K θ_{hf} was in the range 15–20°, and appeared to increase with increasing temperature. This interpretation implies oblique ordering in the intermediate state rather than a mixed $S_\parallel$ and $S_\perp$ order.

The results for $x = 0.007$ have also been published [6], and show that the spin direction is perpendicular to the c-axis, and is along the trigonal x-axis. Magnetic order for this concentration is correctly marked as $S_\perp$ for all temperatures below T_N on the phase diagram in [3].

Our present objective is to use spectra taken with $x = 0.06$ and 0.10 to determine whether the results are consistent with the phase diagram, to successfully analyse the $x = 0.06$ spectra, and to deduce details of the intermediate state. The concentrations chosen lie in the intermediate phase for $x = 0.06$, and close to the boundary between the intermediate phase and the $S_\parallel$ phase for $x = 0.10$. For $x = 0.06$ the spectra in [3] were used, and for $x = 0.10$ we prepared a crystal and collected Mössbauer spectra.

An additional point of interest is the nature of the spin-flopped state. Previous work has suggested that in this state the spin structure is complex [4, 5]. We show for $x = 0.10$ at 5 K that the Mössbauer spectrum is consistent with a simple structure.

2. Experimental details

2.1. $Fe_{0.10}Ni_{0.90}Cl_2$

A single crystal specimen of $Fe_{0.10}Ni_{0.90}Cl_2$ was prepared by the Bridgman–Stockbarger technique [7].Separate preparations of $FeCl_2$ and $NiCl_2$ were mixed in solution, evaporated and heated to 370 °C under continual evacuation, sealed in a quartz tube, and then lowered in a furnace at 1020 °C at 1.4 mm hr^{-1}. Although the nominal iron

concentration was 12 at%, electron-microprobe analysis performed over a number of regions of the crystal showed the mean concentration to be 9.7 at% with a standard deviation of less than 0.3 at%. Unenriched iron was used.

Absorbers were prepared via the sellotape stripping technique in which thin platelets are cleaved perpendicular to the c-axis [8]. Several such platelets are formed into a mosaic mounted on a flat plastic disc for placement in a cryostat, oriented so that the c-axis is parallel to the γ-ray beam.

The γ-ray source was 6 mCi ^{57}CoRh. Because the absorber iron thickness was small, relatively long counting times were necessary (3–21 days per spectrum). A triangular-shaped source velocity waveform was employed; after numerical folding, 500-channel spectra without baseline curvature were obtained. All isomer-shift values in this article are with respect to the centre of the α-Fe spectrum at room temperature.

2.2. $Fe_{0.06}Ni_{0.94}Cl_2$

Spectra of single crystals also cleaved perpendicular to the c-axis are available for $x = 0.06$ at various temperatures [3]. Figure 4 of [3] was photographically enlarged to A3 paper size, taking care to avoid non-linear distortion, and the spectra were digitized with an x–y digitizing tablet. A cubic-spine algorithm was used to convert the data to equally spaced velocity channels to account for any small errors in the digitizing process. The resultant 256-channel spectra were plotted on the same large scale as in the photograph, and compared visually. No discrepancies were present. As a further check two of the spectra were re-digitized, and it was found that operator errors were negligible.

3. Analysis and results

3.1. Thickness saturation and crystallite misalignment

In making single crystal Mössbauer absorbers of metal–dihalide compounds a number of difficulties arise: since the crystals hydrate easily all operations must be done in a dry box; it is difficult to avoid gaps between crystallites which increase the noise component in the spectrum; one cannot be sure how well aligned the crystals are on the holder even though the orientation is such that the γ-ray direction should be close to the c-axis; and finally excessive ^{57}Fe thicknesses lead to saturated line-intensities [6]. The avoidance of holes may be at the expense of greater misalignment.

The absence of significant quantities of hydrated compounds can be readily confirmed by spectra taken above T_N, since the quadrupole splitting in hydrated compounds is relatively large [6].

For paramagnetic single crystal spectra taken with V_{zz} parallel to the γ-ray beam, two lines with an intensity ratio of 3 are expected; however this ratio is reduced by both non-alignment of V_{zz} and thickness saturation. At $T > T_N$ it is almost impossible to distinguish the two effects, since the primary effect of thickness is to saturate line intensities and departure from Lorentzian line shapes is only observed for extreme thicknesses. However, magnetic spectra can be used to distinguish the effects, since thickness saturation reduces as the sub-levels separate by magnetic splitting and affects stronger lines more than weaker lines, whereas the effects of misalignment are constant with temperature.

Thickness saturation was accounted for by multiplying the count computed for each channel by an approximate correction factor [9]:

$$I(T_a) = I(0)[1 - \exp(-\tfrac{1}{2}T_a D_j)J_0(\tfrac{1}{2}iT_a D_j)]^{-1}\tfrac{1}{2}T_a D_j$$

where D_j is the fractional absorption for channel j and T_a was adjustable in least-squares fitting. It was found that the high degree of correlation between T_a and the total absorption D which was also variable resulted in poor convergence, hence the spectral area after applying the correction was adjusted to equal that before applying the correction factor. This procedure successfully removed the dependence.

The average crystallite alignment was determined by varying the polar angles α, β defining the gamma-ray direction with respect to the EFG principal axes. Magnetic order can itself induce non-alignment of V_{zz} with the c-axis, an effect which is discussed in section 3.3. Computation of single crystal spectra was via analytic solution of the full Hamiltonian for the nuclear states [10] with line intensities computed from the appropriate Clebsch–Gordan coefficients and using properties of vector-spherical harmonics in a formulation similar, but not identical, to that in [10] and [11].

For $x = 0.10$ thickness effects were found to be negligible at all temperatures. Several absorbers were prepared and the degree of misalignment was measured from the intensity ration of the quadrupole-split lines in spectra taken at $T > T_N$. The intensity ratio indeed varied between absorbers. Values as high as 2.6 were obtained, but only at the expense of a reasonable signal-to-noise ratio. The absorber used for all low temperature measurements had a ratio of 2.2 at 50 K. This corresponds to an average azimuthal angle α of 23°. In fitting all spectra α was allowed to vary, but was always found to be in the range 18–24°.

For $x = 0.06$ both thickness effects and non-alignment appeared to be present. At 50 K the paramagnetic line intensity ratio is 1.9. Values of α for temperatures below 46 K were in the range 13–17° and T_a was determined to be 2.2(3) (however not that D_j, which is a multiplier of T_a in the thickness correction, was arbitrarily set to a maximum of 0.1 for each digitized spectrum).

3.2. Low temperature results

Spectra for $x = 0.10$ are shown in figure 1. These were fitted assuming that the magnetization is parallel and antiparallel to the c-axis (the $S_\parallel$ state). In this case it follows that the hyperfine magnetic field ($\boldsymbol{B}_{hf}$) is parallel to V_{zz} and hence the hyperfine angles θ_{hf} and ϕ_{hf} defining the direction of $\boldsymbol{B}_{hf}$ with respect to the EFG principal axes are zero, and that the EFG asymmetry parameter η is zero. Hence the parameters allowed to vary in the fit were: α, β (polar angles defining the γ-ray direction with respect to the EFG principal axes), B_{hf}, the quadrupole coupling term $EQ(= \frac{1}{2}eQV_{zz})$, the isomer shift δ, the full linewidth at half maximum intensity Γ, D, and a baseline parameter.

Excellent fits were obtained at all temperatures, as shown by the full lines through the points in figure 1. Reasonably narrow linewidths ($\Gamma \simeq 0.35$ mm s^{-1}) demonstrate that the parameters are not significantly distributed and that all moments are in the $S_\parallel$ state.

Spectra for $x = 0.06$ are shown in figure 2. These were initially fitted assuming a single ferrous site and the direction of the magnetization was allowed to vary. This was an unsatisfactory explanation, even when allowance was made for crystallite non-alignment and thickness saturation. The chief inadequacy of the fits was that the line

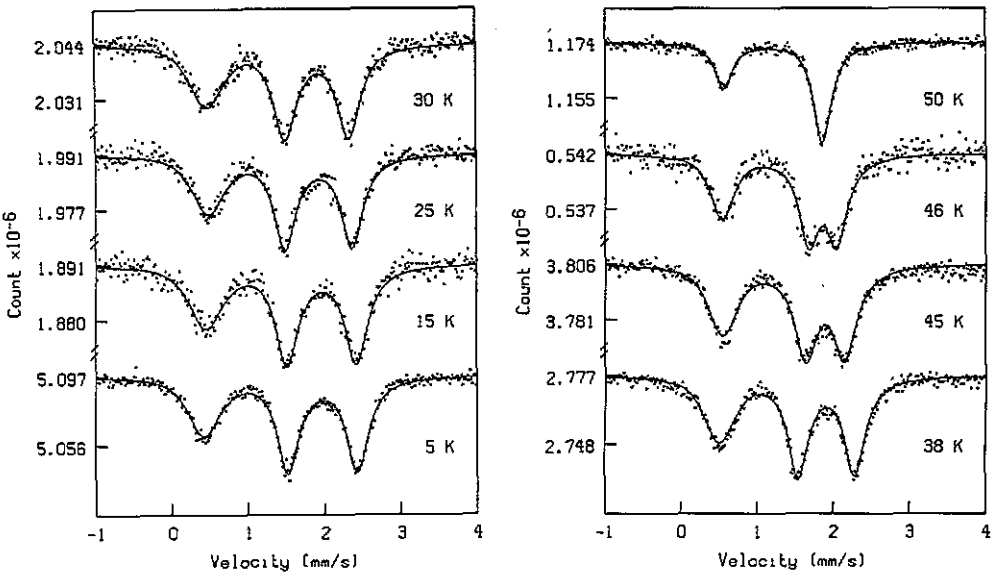

Figure 1. Mössbauer spectra of oriented platelets from a single crystal of $Fe_{0.10}Ni_{0.90}Cl_2$ at the temperatures shown. The same absorber was used for all spectra. The full lines represent the least-squares fit obtained by assuming all the moments are in the $S_{\parallel}$ state.

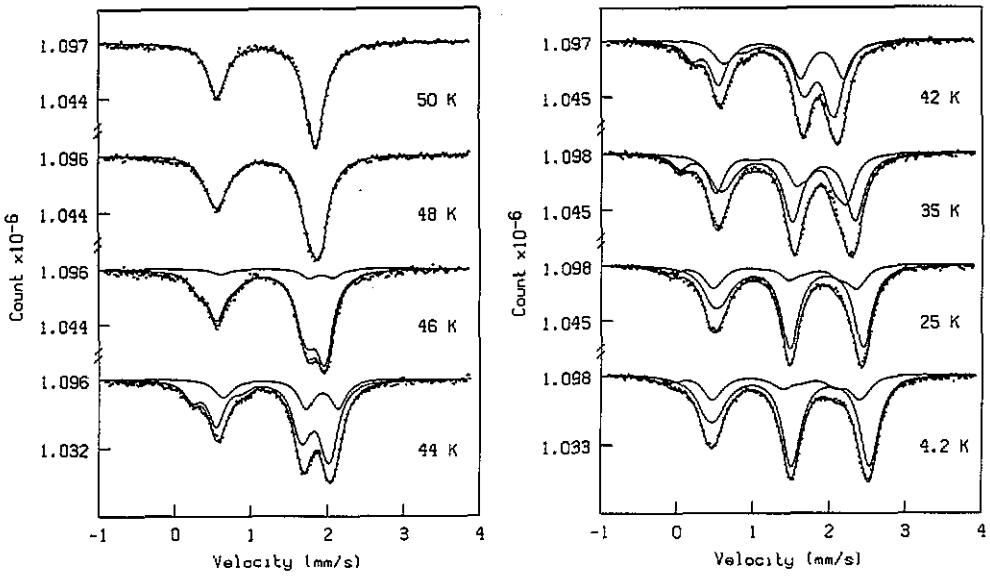

Figure 2. Mössbauer spectra of $Fe_{0.06}Ni_{0.94}Cl_2$ taken by Ito *et al* [3]. Note that the γ-count axis was artificially scaled. The full lines represent moments in the $S_{\parallel}$ and $S_{\perp}$ states, as well as the sum of the subspectra. $S_{\parallel}$ dominates at 4.2 K but decreases to zero in favour of $S_{\perp}$ at temperatures approaching T_N.

at 1.5–1.8 mm^{-1} is too intense to be properly accounted for at 35–44 K by a single site.

Excellent fits (shown in figure 2) were obtained by allowing two ferrous sites, one corresponding to moments in the $S_{\|}$ state and one corresponding to a second state. The parameters for the first site were as for $x = 0.10$. The proportion of $S_{\|}$ spins was determined from the relative areas of the two subspectra, and is plotted as a function of temperature in figure 3. It is 0.74 at 4.2 K, and decreases smoothly to zero at $T_N = 49$ K. The linewidths (Γ) were narrow (0.24–0.35 mm s^{-1}) for both sites.

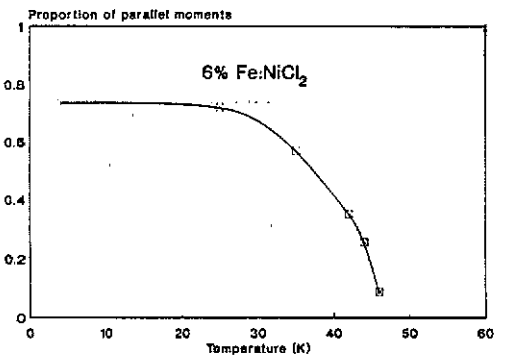

Figure 3. The proportion of spins in $S_{\|}$ (the other spins are in $S_{\perp}$) for $Fe_{0.06}Ni_{0.94}Cl_2$. the curve is drawn as a guide to the eye.

For the second site a full set of hyperfine parameters including θ_{hf}, ϕ_{hf} and η was varied. In general, the parameter set B_{hf}, EQ, θ_{hf}, ϕ_{hf} and η is undetermined since there are only four $I = \frac{3}{2}$ state sublevels. The splitting of the $I = \frac{1}{2}$ ground state, which has zero quadrupole moment, allows unambiguous determination of B_{hf} and the quantity $QS = EQ(1 + \eta^2/3)^{1/2}$ is unambiguous [12]. After finding one set of hyperfine parameters, other compatible sets were computed from the equations for the coefficients in the secular equation for $I = \frac{3}{2}$ [12]. At all temperatures θ_{hf} was in the range 82–89° and ϕ_{hf} less than 10°. Allowed ranges in the other parameters were small. These results are characteristic of $S_{\perp}$ order, as shown in section 3.3.

A very small, but statistically significant, discrepancy between the experimental and calculated curves is noticeable near 0 mm s^{-1} at 42–48 K in figure 2. This is consistent with the presence of trace impurities of hydrated compounds (iron-doped $NiCl_2.nH_2O$ where n is an integer), which order below 35 K [6]. The intensity of lines in a Mössbauer spectrum decrease rapidly on cooling below the ordering temperature. Hydrated compounds would therefore be most noticeable at 42–48 K, since in this region the impurities are paramagnetic and the anhydrous material is magnetically ordered. Alternatively, the discrepancy might indicate a more complex magnetic order for a very small proportion of moments, even though it is apparent that fitting only two magnetic sites provides very good overall agreement.

3.3. Temperature dependence of Mössbauer parameters and crystal field analysis

A crystal field model was used to confirm that the identification of $S_{\|}$ and $S_{\perp}$ order is consistent with the temperature variations of both B_{hf} and QS. The procedure has

been described in detail [6]; briefly, the ^5D term of Fe^{2+} is split by a cubic field giving a $^5T_{2g}$ wavefunctions are perturbed by

$$\mathcal{H} = \Delta[L_z^2 - \tfrac{1}{3}L(L+1)] + \lambda \boldsymbol{L}\cdot\boldsymbol{S} + J_{\text{eff}}\langle S_i\rangle(S_x\cos\phi_{\text{ex}}\sin\theta_{\text{ex}} + S_y\sin\phi_{\text{ex}}\sin\theta_{\text{ex}} + S_z\cos\theta_{\text{ex}})$$

where Δ, λ and J_{eff} are respectively trigonal field, spin–orbit and exchange interaction constants to be determined. The direction of magnetization is defined by the polar angles $\phi_{\text{ex}}, \theta_{\text{ex}}$ with respect to the trigonal crystallographic axes. Diagonalization of $\mathcal{H}$, and use of Boltzmann statistics, allows calculation of the hyperfine magnetic field which is the sum of orbital, Fermi contact, and dipolar contributions:

$$\boldsymbol{B}_{\text{hf}} = (1/2\pi)\mu_0\mu_{\text{B}}\langle r^{-3}\rangle\boldsymbol{L} + \tfrac{1}{2}\boldsymbol{B}_{\text{c}}\boldsymbol{S} + (1/84\pi)\mu_0\mu_{\text{B}}\langle r^{-3}\rangle[\tfrac{3}{2}\boldsymbol{L}(\boldsymbol{L}\cdot\boldsymbol{S}) + \tfrac{3}{2}(\boldsymbol{L}\cdot\boldsymbol{S})\boldsymbol{L} - \mathrm{L}(\mathrm{L}+1)\boldsymbol{S}]$$

where $\langle r^{-3}\rangle$ and B_{c} are constants to be determined. Components of the valence contribution to the electric field gradient are given by

$$V_{zz}^{\text{latt}} = (1/42\pi\epsilon_0)|e|\langle r_Q^{-3}\rangle[\tfrac{3}{2}(L_iL_j + L_jL_i) - \delta_{ij}L(L+1)].$$

A small lattice contribution to the EFG was also included:

$$V_{zz}^{\text{latt}} = -2V_{yy}^{\text{latt}} = -2V_{xx}^{\text{latt}} = 14\Delta(1-\gamma)/e\langle r^2\rangle$$

where the free-ion values $\langle r^2\rangle = 1.4$ au and $(1-\gamma) = 12$ were used [13] and references therein). The principal values of $\boldsymbol{V}^{\text{val}} + \boldsymbol{V}^{\text{latt}}$ enable calculation of EQ and η, and expressing $\boldsymbol{B}_{\text{hf}}$ in terms of the principal EFG axes gives θ_{hf} and ϕ_{hf}.

Least-squares fitting was used to simultaneously fit calculated and measured B_{hf} and QS values as a function of temperature. The variable parameters were T_{N}, J_{eff}, B_{c}, $\langle r^{-3}\rangle$, $\langle r_{\text{Q}}^{-3}\rangle$, Δ and λ. The azimuthal polar angle (θ_{ex}) defining the direction of the magnetization was fixed at 0° and 90° for $S_{\parallel}$ and $S_{\perp}$ respectively.

For $S_{\perp}$ in $x = 0.06$ the magnetization was assumed to lie along the trigonal x-axis, which is the case for $x = 0.007$ [6].

Table 1. Parameters for $Fe_xNi_{1-x}Cl_2$ determined by least-squares fitting B_{hf} and QS with the crystal field model.

x	State	T_{N} (K)	J_{eff} (cm^{-1})	B_{c} (T)	$\langle r^{-3}\rangle$ (au)	$\langle r_{\text{Q}}^{-3}\rangle$ (au)	Δ (cm^{-1})	λ (cm^{-1})
0.007[a]	$S_{\perp}$	52(1)	−24(1)	−40(2)	3.9(2)	3.6(3)	−74(7)	−83(5)
0.06	$S_{\perp}$	49(1)	−20(1)	−38(2)	3.8(2)	3.9(3)	−71(10)	−93(8)
0.06	$S_{\parallel}$	49(1)	−69(20)	−50(3)	4.0(2)	3.2(3)	−65(10)	−108(8)
0.10	$S_{\parallel}$	46(1)	−43(10)	−50(3)	4.0(2)	3.3(3)	−89(8)	−91(6)

[a] Data from [6].

The crystal field parameters obtained are listed in table 1, and the calculated and experimental Mössbauer values are plotted in figures 4 and 5. It can be seen that good agreement was obtained for B_{hf}, and moderate agreement for QS. Contributions

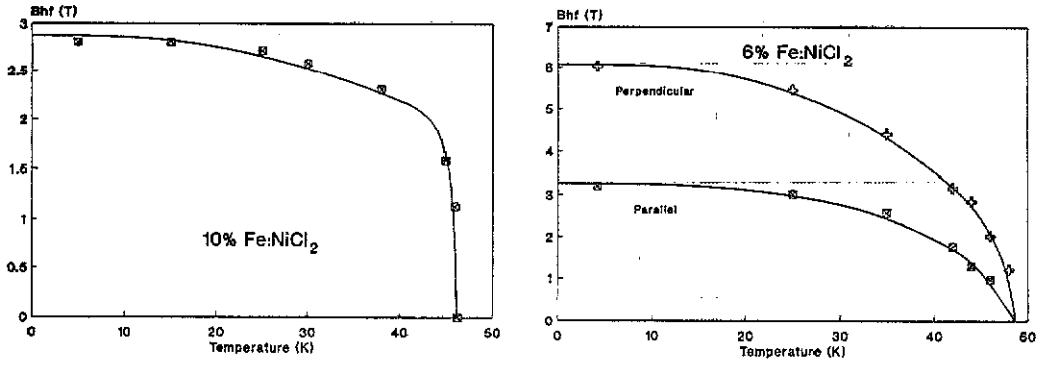

Figure 4. Crystal field fits to B_{hf} for $x = 0.10$ and 0.06. For $x = 0.06$ separate curves are shown for $S_{\|}$ and $S_{\perp}$.

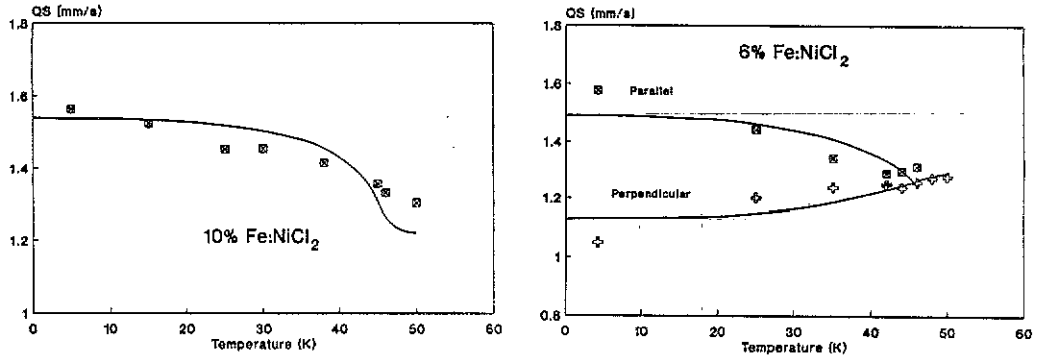

Figure 5. Crystal field fits to the temperature variations of $QS[= \frac{1}{2}eQV_{zz}(1 + \eta^2/3)^{1/2}]$.

to QS from the lattice are not reliably known, and it appears from figure 5 that for $x = 0.10$ these may have been somewhat underestimated since the temperature variation of QS is not as large as calculated. For the $S_{\|}$ states it was found that the goodness of fit was not particularly sensitive to J_{eff}, and consequently the uncertainty in the values obtained is relatively large.

In the $S_{\|}$ state the magnetization tilts the EFG principal axes such that α, the angle between V_{zz} and the trigonal z-axis, is about 12° at low temperatures. This effect helps explain the values of 13–17° determined by fitting the spectra, although some physical misorientation of crystallites may also be present. For $S_{\|}$ there is no such tilting effect, and physical misalignment is the only contribution to α.

3.4. Applied field spectrum, $x = 0.10$

The spectrum in figure 6 shows the effect of a 6 T magnetic field applied parallel to the γ-ray direction for $Fe_{0.10}Ni_{0.90}Cl_2$ at 5 K. The absorber was the same as that used to collect the data in figure 1. A single ferrous site was assumed in least-squares analysis of the spectrum, and the direction of $\boldsymbol{B}_{hf}$ was allowed to vary. A good fit was obtained, as shown by the full line in the figure, with the parameters B_{hf} =

9.9(1) T, $EQ = 1.57(4)$ mm s^{-1}, $\eta = 0.1(1)$, $\theta_{hf} = 30(5)°$, and $\phi_{hf} = 17(20)°$, where the uncertainties in each parameter were estimated by fitting the spectrum with only that parameter varying. The linewidth ($\Gamma = 0.40(2)$ mm s^{-1}) was somewhat broader than in the 5 K zero-field spectrum (0.35(2) mm s^{-1}; however, this is attributable to, and consistent with, the fringing magnetic field (0.2 T) at the source position.

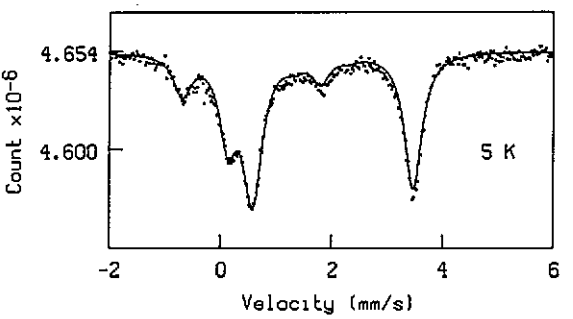

Figure 6. Mössbauer spectrum of $Fe_{0.10}Ni_{0.90}Cl_2$ at 5 K with a 6 T magnetic field applied along the γ-ray direction. The full curve was obtained assuming a single ferrous site.

Ranges of parameters resulting from the under-determination of the Mössbauer spectrum were computed as for the zero-field spectra. It was found that θ_{hf} ranges between 23–30° including uncertainties), EQ is 1.43–1.57 mm s^{-1}, and that wide ranges of η (0.1–0.8) and ϕ_{hf} (0–90°) were allowed. Hence the set of fitted parameters is one of an infinity of sets giving the identical Mössbauer spectrum. The value of QS is (unambiguously) measured to be 1.57(4) mm s^{-1}, and is consistent with the zero-field value of 1.56(4) mm s^{-1}. The values of θ_{hf} and Γ indicate that the ferrous spins are equivalently canted with respect to the c-axis. The most likely explanation is that an applied field of 6 T induces a spin-flopped phase, and that the moments have been substantially drawn back towards the c-axis.

4. Conclusions

Mössbauer spectra of $Fe_xNi_{1-x}Cl_2$ ($x = 0.10$ and 0.06) have been satisfactorily analysed. For $x = 0.10$ the results are consistent with $S_{\|}$ order at all temperatures below $T_N = 46$ K. For $x = 0.06$ the $S_{\|}$ and $S_{\perp}$ phases coexist at 4.2 K, but as the temperature is raised to $T_N = 49$ K the proportion of spins in $S_{\|}$ decreases to zero. Oblique antiferromagnetic phases are absent. The spin-flopped state of $x = 0.10$ at 5 K can be characterized by a single ferrous site.

Crystal field analysis of the Mössbauer parameters confirmed the magnetic phase identification, and showed that the exchange at ferrous sites was substantially greater for $S_{\|}$ than for $S_{\perp}$.

Acknowledgments

We are grateful to S Bocquet and J D Cashion for helpful comments.

References

[1] Howes B D, Price D C and Wiltshire M C K 1984 *J. Phys. C: Solid State Phys.* **17** 3669–84
[2] Ito A 1986 *Hyperfine Interact.* **27** 81–92
[3] Ito A, Tamaki T, Someya Y and Ikeda H 1983 *Physica* B **120** 207–11
[4] Ito A, Kitazawa M, Tamaki T, Morimoto S, Torikai E, Goto T and Sakakibara T 1985 *Abstracts of the Int. Conf. on the Applications of the Mössbauer Effect* (Belgium: Katholieke Universiteit Leuven) abstracts, p2.46
[5] Ito A, Torikai E, Kitazawa M, Tamaki T, Goto T, Sakakibara T, Todo S and Oguro I 1986 *J. Magn. Magn. Mater.* **54–7** 39–40
[6] Pollard R J, McCann V H and Ward J B 1982 *J. Phys. C: Solid State Phys.* **15** 6807–22
[7] Pollard R J 1982 *J. Cryst. Growth* **60** 153–4
[8] Campbell J A 1978 *J. Phys. C: Solid State Phys.* L **11** 795–7
[9] Margulies S and Ehrman J R 1961 *Nucl. Instrum. Methods* **12** 131–7
[10] Häggström L 1974 *Institute of Physics Report* UUIP–851 (Sweden: University of Uppsala)
[11] Hoy G R and Chandra S 1967 *J. Chem. Phys.* **47** 961–5
[12] Pollard R J, McCann V H and Ward J B 1983 *J. Phys. C: Solid State Phys.* **16** 345–53
[13] Ingalls R 1964 *Phys. Rev.* A **133** 787–95